Since January 2020 Elsevier has created a COVID-19 resource centre with free information in English and Mandarin on the novel coronavirus COVID-19. The COVID-19 resource centre is hosted on Elsevier Connect, the company's public news and information website.

Science of the Total Environment 752 (2021) 141928

Contents lists available at ScienceDirect

Science of the Total Environment

journal homepage: www.elsevier.com/locate/scitotenv

Understanding ozone pollution in the Yangtze River Delta of eastern China from the perspective of diurnal cycles

Jiawei Xu, Xin Huang *, Nan Wang, Yuanyuan Li, Aijun Ding

School of Atmospheric Sciences, Nanjing University, Nanjing 210023, China
Collaborative Innovation Center of Climate Change, Jiangsu Province, Nanjing 210023, China

HIGHLIGHTS

- Cluster analysis of ozone episodes sheds lights on its causes.
- Mixed anthropogenic and biogenic emissions enhance ozone photochemical pollution.
- Sea-land breeze promotes ozone accumulation in coastal cities in the YRD.

GRAPHICAL ABSTRACT

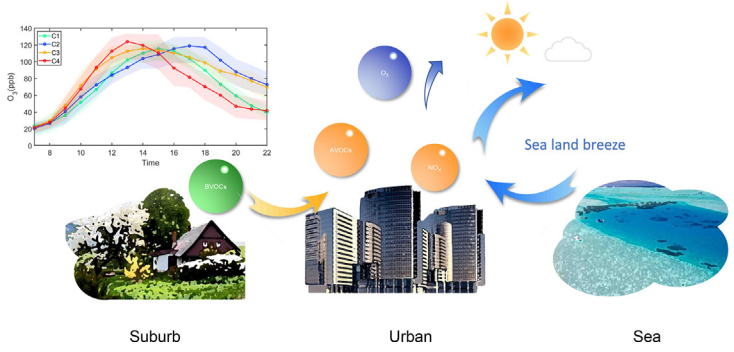

ARTICLE INFO

Article history:
Received 10 July 2020
Received in revised form 22 August 2020
Accepted 22 August 2020
Available online 22 August 2020

Editor: Jianmin Chen

Keywords:
Ozone pollution
YRD
Cluster analysis
Biogenic emissions
Sea-land breezes

ABSTRACT

Ozone (O_3) pollution has aroused increasing attention in China in past years, especially in the Yangtze River Delta (YRD), eastern China. Ozone and its precursors generally feature different diurnal patterns, which is closely related to atmospheric physical and chemical processes. This work aims to shed more light on the causes of ozone pollution from the perspective of the diurnal patterns. Hundreds of ozone pollution days (with maximum hourly O_3 concentration over 100 ppb) during 2013–2017 were identified and then clustered into 4 typical types according to the diurnal variation patterns. We found that ozone pollution in Shanghai was particularly severe when anthropogenic pollutant mixed with biogenic volatile organic compounds (BVOCs) under the prevailing southwesterly wind in summer. The reason could be attributed to the spatial disparities of ozone sensitivity regime in YRD: VOC-limited regime around in the urban area and NO_x-limited regime in the rural forest regions in the southern and southwest. The transition of sensitivity regimes along south/southwest wind tended to promote the photochemical production of ozone, making daily O_3 pollution time exceeding 6 h of the day. In addition, ozone peak concentration in Shanghai was highly dependent on the evolution of sea-land breezes (SLBs). Earlier sea breeze associated with approaching typhoon in the West Pacific caused less cloud (−25%) and more solar radiation (11%) in YRD, which subsequently led to a rapid increase of O_3 concentration in the morning and a deteriorated ozone pollution during noon and the afternoon. This study highlights the importance of observation-based processes understanding in air quality studies.

1. Introduction

Tropospheric ozone (O_3), which exerts adverse impacts on human health and ecosystem productivity, has attracted increasing attention globally (Bosson et al., 2007; Brauer et al., 2016; Buckley et al., 1975;

* Corresponding author at: School of Atmospheric Sciences, Nanjing University, Nanjing 210023, China.
E-mail addresses: xinhuang@nju.edu.cn (X. Huang), dingaj@nju.edu.cn (A. Ding).

https://doi.org/10.1016/j.scitotenv.2020.141928
0048-9697/

Ding et al., 2013b; Tager et al., 2005; Uysal and Schapira, 2003; Xue et al., 2020). Moreover, tropospheric ozone also acts as an effective greenhouse gas and thus also influences global climate change (IPCC, 2013; Seinfeld and Pandis, 2012). As one of the most important sources of the hydroxyl radical, it is of great importance with regard to atmospheric chemistry (Atkinson, 2000). Tropospheric ozone mainly forms through photochemical reactions of volatile organic compounds (VOCs), methane (CH_4), carbon monoxide (CO) and nitrogen oxides ($NO_x = NO + NO_2$) (Chameides et al., 1992; Sillman, 1995). In recent decades, many studies suggested notable increases in tropospheric ozone, which were mainly attributed to fast-growing anthropogenic emissions as well as climate warming (Cooper et al., 2010; Lelieveld et al., 2004).

Though emission and climate variability determine ozone trend, synoptic conditions play a dominant role in day-to-day ozone variation and pollution episodes, such as typhoon (Ding et al., 2004; Jiang et al., 2008; Shu et al., 2016; Zhang et al., 2013), anticyclone (He et al., 2012; Tie et al., 2009; Xu et al., 2017), and sea-land breezes (SLBs) (Bouchlaghem et al., 2007; Ding et al., 2004; Klemm et al., 1998; Lasry et al., 2005; Stauffer et al., 2015). For example, a typhoon in West Pacific has been proven to make SLB delay and lower mixing height in the Pearl River Delta, causing ozone concentrations more than 150 ppb in these areas (Ding et al., 2004; Zhang et al., 2013). Meso-scale anticyclone conditions have been indicated to contribute the accumulation of ozone precursors and subsequently impact ozone concentration (Xu et al., 2017). In coastal areas, the penetration of sea breeze systems into land would form sea breeze convergence zone, resulting a high ozone level (Ding et al., 2004; Liu et al., 2002; Mangia et al., 2010). SLBs circulation might also exert significant on transporting ozone pollution along the coasts (Adame et al., 2010; Ding et al., 2004; Stauffer et al., 2015).

The eastern China, as one of the most densely-populated and rapidly-developing region across the world, has been suffering from fine particle ($PM_{2.5}$) and ozone pollution in past decades (Ding et al., 2013b). Owing to the strict national-wide emission control since 2013, China has witnessed a fast drop of $PM_{2.5}$ concentration in recent years (Ding et al., 2019; Zhang et al., 2019). However, ozone pollution is getting increasingly severe and arouses the concerns from both the government and the public, particularly in developed regions like the Yangtze River Delta (YRD) region (Huang et al., 2020a; Li et al., 2018; Wang et al., 2020). The highest ozone concentration often occurs from May to July in the YRD region, with maximum daily 8-hour average (MDA8) ozone trend of 2.3 ppb $year^{-1}$ for 2013–2017 (Li et al., 2018; Wang et al., 2017).

Shanghai, a megacity located in the east part of China, has developed into an international metropolis in the past decades. Being the largest city of the YRD region, Shanghai also faced extreme ozone pollution events (Huang et al., 2014; Kong et al., 2018; Ming et al., 2017; Pathak et al., 2009). The increasing trend of daily maximum O_3 concentration reached more than 1.3 ppb $year^{-1}$ from 2006 to 2015, mostly affected by VOCs emissions (Geng et al., 2008; Xu et al., 2019). There have been several studies on determining VOC-limited regime in the Shanghai region (Geng et al., 2008; Jin and Holloway, 2015; Li et al., 2011; Tie et al., 2013; Wang et al., 2019). In general, in the VOC-limited regime, the increments of VOCs raise ozone concentration (Sillman and He, 2002; Sillman et al., 2003; Sillman and West, 2009). Since there are massive forests around Shanghai (particularly in the southwest to the city), not only anthropogenic emissions but also biogenic VOCs (BVOCs), like isoprene (C_5H_8), promoted ozone production in these areas (Li et al., 2016; Liu et al., 2018; Wei et al., 2007). For instance, Geng et al. (2011) pointed out that BVOCs emitted in forest areas promoted ozone pollution in Shanghai by regional transport. In addition, meteorological conditions like SLBs have been suggested to play an important role in the occurrence of ozone pollution in Shanghai due to the vicinity of the East China Sea. Tie et al. (2009) found that when the subtropical high was weak, resulting in weak breeze in the YRD region, making SLBs easy to form. Ozone was trapped inside the city due to SLBs, leading to high ozone concentration in Shanghai.

This work focuses on the analysis of ozone pollution characteristics in Shanghai mainly based on in-situ observational data with a focusing on their diurnal patterns and peak concentrations. The rest of this paper is structured as follows. The datasets and methods are described in Section 2. Section 3 gives the results from K-means clustering and analyzes the effects of regional transport as well as sensitivity regime. The mechanisms of ozone formation under the influence of SLB are also discussed. Conclusions are summarized in Section 4.

2. Data and methods

2.1. Observational and reanalysis data

Ground-based observations of O_3, nitrogen dioxide (NO_2) and CO concentration at more than 1500 stations since 2013 are archived at the air monitoring data center of the Ministry of Ecology and Environment of China. The monitoring networks covered most parts of China, and stations were particularly concentrated in the YRD region. As severe ozone pollution events that jeopardized human bodies and agriculture production mostly occurred in summer (Meleux et al., 2007; Wang et al., 2017; Zhang et al., 2014), its concentrations records from 2013 to 2017 between June and August were selected in this study, with valid measurement data >90%. In addition to air pollutants, meteorological parameters were recorded by China's meteorological observing networks. The sites data measured included hourly wind speed and direction, air temperature, humidity and air pressure. Based on these datasets, the photochemical and physical impacts of meteorological factors to ozone were analyzed.

The fifth generation European Centre for Medium-Range Weather Forecasts (ECMWF) atmospheric reanalysis of the global climate (ERA5) data was used as ancillary data due to the lack of radiation and meteorological measurements in the sea. With the same time period and interval as observed data, it provided meteorological variables such as mean sea level pressure, 2 m-temperature and 10 m-wind at $0.25° \times 0.25°$ grid. Apart from these data, daily formaldehyde (HCHO) and NO_2 column densities were obtained from the resolution of the GOME-2 retrievals. The data was averaged to $0.25° \times 0.25°$ grids to match the ERA5 data. It should be noted that pixels with more than 40% cloud fraction were filtered out (Boersma et al., 2004). A detailed description on GOME-2 column density can be found in Boersma et al. (2004) and De Smedt et al. (2008).

2.2. WRF-Chem simulation and source identification calculation

The calculations of BVOCs emissions in YRD presented in this study were performed using the version 3.7 of Weather Research and Forecast Model with Chemistry (WRF-Chem3.7). This modeling system includes a dynamical and a chemical module, simulating meteorology-chemistry-aerosol-radiation-cloud interactions via direct, semi-direct and indirect effects (Grell et al., 2005). The dynamical module, known as WRF, is a mesoscale numerical weather prediction system designed for operational forecasting and atmospheric research. In addition to dynamical calculations, a chemical module is coupled on-line with the WRF model for simulating BVOCs and other chemicals. Inside the model, biogenic emissions are generated by Model of Emissions of Gases and Aerosols from Nature (MEGAN) developed by Guenther et al. (2007), which was wildly used in simulation of BVOCs in China (Fu and Liao, 2012; Li et al., 2015; Liu et al., 2018; Situ et al., 2013; Tie et al., 2013; Tie et al., 2009). A detailed description of WRF-Chem can be found on the website https://ruc.noaa.gov/wrf/wrf-chem/. In this study, the model domain covered East China and its surrounding area, centered at 35.0°N, 110.0°E with a grid resolution of 20 km. National Center for Environment Prediction (NCEP) global final analysis data (FNL) was used as the initial and lateral boundary conditions of meteorological variables with a $1° \times 1°$ spatial resolution that update every 6 h. The simulations were conducted from 1st June to 31st August in

2013–2017. For all the simulation runs, the first 6 days integration every year was considered as model spin-up.

Long-range transport under specific synoptic weather plays an important role on air quality (Huang et al., 2020b; Zhang et al., 2016; Zhang et al., 2013). To investigate the effects of regional transport, Lagrangian particle dispersion modeling (LPDM) was used. The model was based on Hybrid Single-Particle Lagrangian Integrated Trajectory (Hysplit) which was extensively applied for modeling mass trajectory, diffusion and deposition (Draxier and Hess, 1998; Stein et al., 2016). The model began when certain particles were released at a point. After that, the Lagrangian method was used for the calculation of advection and diffusion of the particles, and the Euler method was used for the calculation of the concentration portion. The positions of the particles in the forward or backward transport of the release height over time were calculated by using the averaged wind and turbulent transport, with a simulated maximum time resolution of 1 h. Detailed information of the LPDM can be found in Stein et al. (2016) and Ding et al. (2013a). On account of the advantages of stability and traceability, the LPDM model has been widely used in atmospheric environment research (Ding et al., 2013a; Huang et al., 2016; Xu et al., 2017). In this paper, 3000 particles were released at 100 m and run 24 h backwardly over the Jing'an site (121.425°E, 31.226°N), Shanghai. The residence time of particles at 100 m was identified as the footprint retroplume.

2.3. Clustering of O_3 diurnal pattern

Cluster analysis is a method to find patterns in data without a priori information on the data. As one of clustering algorithms, K-means clustering starts analysis after the number of clusters is already known (Everitt et al., 2011). Founded by MacQueen (1967), K-means clustering analysis classifies n points of data X into initializing k clusters:

$$J = \sum_{k=1}^{k} \sum_{i=1}^{n} \|x_i - u_k\|^2$$

where u is the mean of points in every clusters (the center point within-cluster) and J is the minimum distance from every point to its center point within-cluster. This process is repeated until each cluster is stable. This algorithm is widely used in pollution studies, especially in cases that a priori information on the possible clusters is available (Adame et al., 2012; Austin et al., 2013; Domínguez-López et al., 2014; Jin et al., 2011; Vargas et al., 2015; Zhang et al., 2016).

In this study, cluster analysis was used to investigate different diurnal patterns of ozone during the daytime and early night (7:00–22:00) since that this time period features most peak values of concentration and most obvious ozone variations, while the change in ozone concentration around 00:00–06:00 is relatively small. The ozone concentrations were normalized by Min-Max Feature scaling to bring all values between 0 and 1. Therefore, the diurnal time series of normalized ozone were performed by K-means clustering analysis. A first step for clustering was to define the optimal number of clusters that would be used for following discussion. In this study, groups with a number of clusters between 2 and 7 have been performed. If the number of clusters was larger than 4, some clusters were not showing an obvious difference in diurnal cycles. On the other hand, if 3 or less clusters were selected, some interesting features might be ignored. Finally, the optimal cluster number was 4. After that, each day would be divided into one group. At each iteration, the algorithm divided two days with similar peak into a group. The group number had become less at each iteration until it reached preset value. It was considered that the diurnal patterns in each cluster were similar after the calculation stopped. In this way, we classified the hourly evolution of ozone and study meteorological changes in every cluster after selecting the cluster number. It should be pointed out here that K-means method also has limitations in determining relationship between clusters and transport patterns because different transport patterns may lead to similar ozone patterns.

3. Results and discussions

3.1. O_3 pollution in the YRD region and its diurnal characteristics

Fig. 1 shows the 5-year average (2013–2017) values of summer daily maximum ozone concentrations in the YRD region from the air-quality monitoring networks in eastern China. As Shanghai accommodates more than 24 million residents and assembles many industrial plants, it was not surprised that the most polluted areas were around Shanghai. The spatially highest concentrations were between Shanghai and Jiaxing, reaching up to 90 ppb, and the average daily peak concentrations in downtown Shanghai exceeded 80 ppb. The ozone trends were 2.44 ppb year^{-1} in Shanghai and 0.83 ppb year^{-1} in Jiaxing in summer. In contrast, concentrations in northern cities, such as Suzhou and Wuxi, were approximately 75 ppb. In-situ concentrations were only around 70 ppb in farther cities like Hangzhou, with increasing rate about 1.05 ppb year^{-1} due to less population and industrial activities.

As a station in the urban area of Shanghai, the Jing'an monitoring station was selected for further analysis due to its long time span and high data quality (Fig. 1). The Chinese National Ambient Air Quality Standard for maximum hourly ozone concentration is 100 ppb at 298 K and 1013 hPa, and accordingly 111 ozone pollution days were identified and performed with K-means cluster analysis. The diurnal clustering patterns of ozone and their numbers in June–August are shown in Fig. 2. The ozone concentrations of all clusters were relatively low before

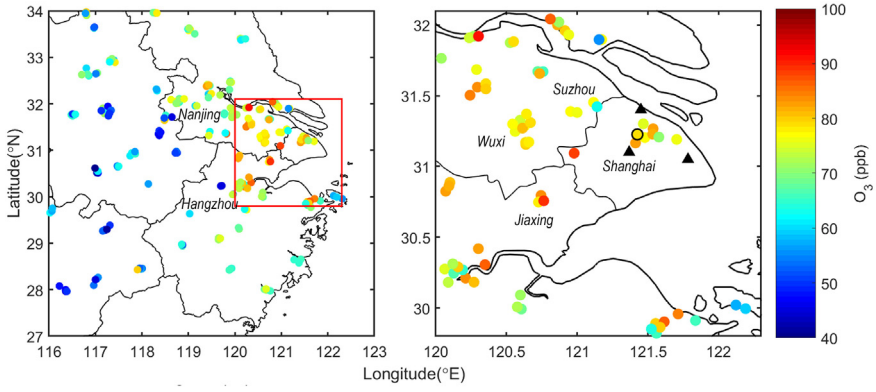

Fig. 1. Mean values of the daily maximum ozone concentration in summer from 2013 to 2017. The black open circle represents Jing'an station and three solid black triangles represent meteorological stations.

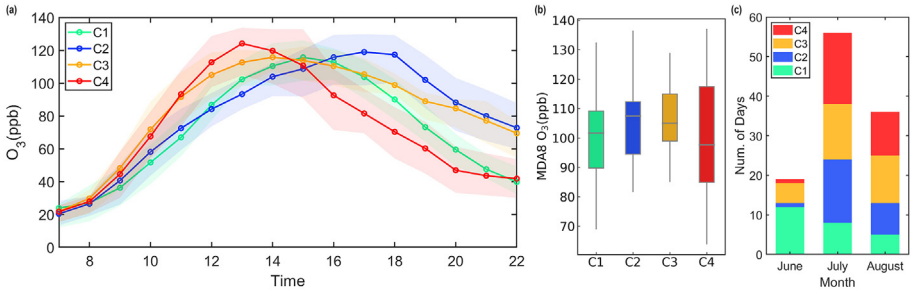

Fig. 2. (a) Diurnal patterns of ozone concentration of different clusters in Shanghai. Lines and shadows show mean value and 25th and 75th percentiles, respectively. (b) Boxplot of maximum daily 8-h average (MDA8) ozone concentration of different clusters. Note that the vertical lines for each box correspond to the maximum and minimum values, and the boxes and the horizontal lines mark the 25th, 75th, and 50th percentiles, respectively. (c) Days of four clusters in different months in summer.

9:00 local solar time (LST) due to weak photochemical reactions. Then all clusters underwent ozone pollution during daytime with different peak time. Among them, C1 (Cluster 1) mainly occurred in June, peaking between 14:00 LST and 16:00 LST. C3 (Cluster 3) featured a longer time duration of ozone pollution and higher MDA8 ozone concentration, being frequent in July and August. The diurnal pattern defined as C2 (Cluster 2), mostly occurring in July, usually showed pollution around sunset. The ozone concentration of C4 (Cluster 4) rose rapidly after sunrise in comparison to other clusters. The average increase rates reached 25.72 ppb h^{-1} at 12:00 LST, of the fastest speed within all the four clusters. The last group occurred mostly in July.

Meteorological conditions have been indicated to play important roles in ozone pollution (Ding et al., 2004; Ding et al., 2013b). When ozone pollution got severe, the Pacific High was located to the southeast direction of Shanghai in summer (Fig. 3a). At the edge of the subtropical high, the daytime wind was often southwesterly in downtown (Fig. 3b). The stagnant conditions associated with the Pacific High cause strong downward radiation and little cloud cover, which was quite favorable for the photochemical production and accumulation of ozone in these regions.

As ozone precursors, NO_x were mainly emitted in cities with a large combustion of fossil fuel while VOCs had both anthropogenic and biogenic sources. Fig. 3c shows the land-use types in the YRD region. There were dense cities and towns in Shanghai and the northern areas, with intensive anthropogenic VOCs (AVOCs) and NO_x emissions. Meanwhile, areas south to Shanghai are characterized by a great deal of forests emitting BVOCs. The geographical location determines that ozone concentration in Shanghai was affected by different effects at different times in summer, which would be discussed in detail in following parts. Since that southwesterly occurred frequently in summer time, VOCs emissions from southeast areas such like Hangzhou might be transported to Shanghai, leading high ozone concentration. The phenomenon was also discussed in previous studies (Geng et al., 2011; He et al., 2012).

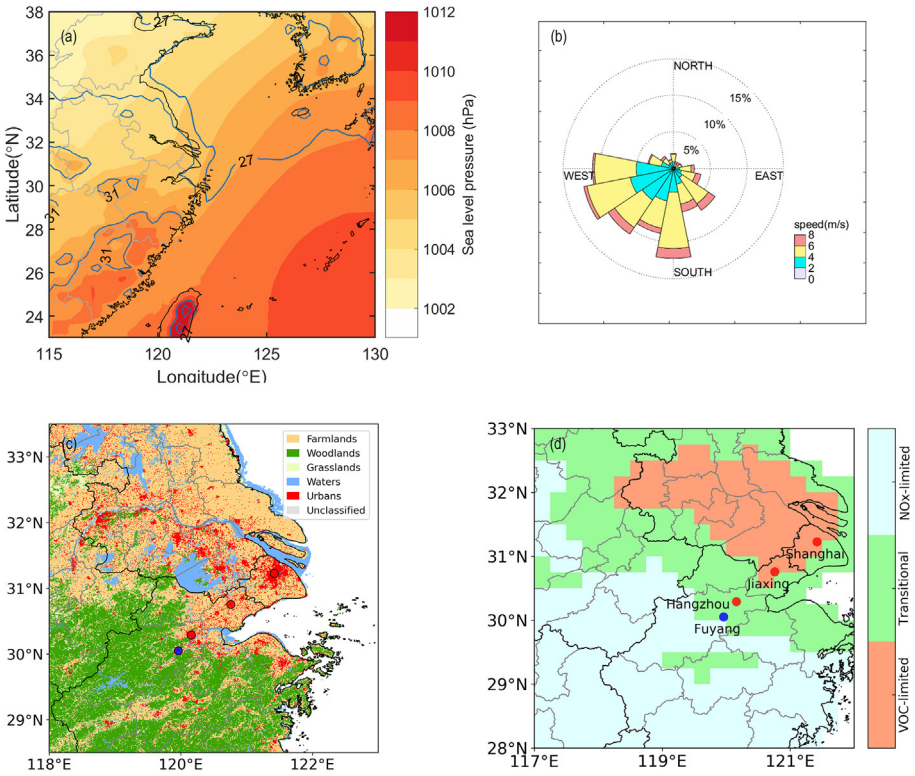

Fig. 3. (a) Mean Sea level pressure and isotherms in western Pacific and (b) wind rose in Shanghai during day time (8:00–18:00) in summer. (c) Landsat 8 satellite-retrieved land-use maps of the YRD region. (d) Sensitivity regimes defined by satellite data of the YRD region in summer. The red dots represent urban station, while the blue dot represents suburb station.

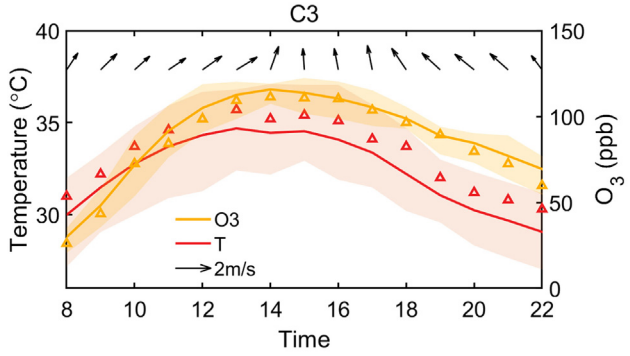

Fig. 4. Time series of 2-meter temperature and 10-meter wind of C3 in Shanghai. Lines and triangles show mean and median values. Shadow areas present 25th–75th data ranges.

Since that the land use types in the southwest areas were different from that in Shanghai, the regional transport might have experienced a shift in the sensitivity regimes. In this study, ratios of satellite column concentration were used as an indicator of ozone sensitivity regimes (Martin et al., 2004). This method can figure out sensitivity regime in places lacking observation data. The ratio of $HCHO/NO_2$ has been wildly used to investigate the ozone sensitivity regime in previous studies (Choi et al., 2012; Duncan et al., 2010; Jin et al., 2017; Jin and Holloway, 2015; Sillman, 1995). $HCHO/NO_2$ ratios below 1 are considered as VOC-limited regime; $HCHO/NO_2$ ratios above 2 reflect NO_x-limited regime; and $HCHO/NO_2$ ratios between 1 and 2 indicate transitional regime. Fig. 3d shows ozone sensitivity regime defined by the average ratio of the column concentration of $HCHO/NO_2$ in summer. The dots are the locations of environmental stations. The red dots represent urban station, while the blue dot represents suburb station. In general, Shanghai and its northwest areas were close to the VOC-limited regime but mostly in transitional regime. Comparatively, the southwest areas gradually converted to NO_x-limited regime because of vast woodlands and the associated intensive BVOC emission. Though the satellite retrieval is just indicative of sensitivity regimes around overpass time (9:30 LST), the sensitivity regimes is demonstrated to change from VOC-limited to transitional regime according to the diurnal variation in Wang et al. (2019). Therefore, ozone chemical sensitivity tends to be a more transitional regime in afternoon compared with the diagnosis derived from satellite observed $HCHO/NO_2$ ratios in the morning.

3.2. Ozone enhancement due to regional transport and change of sensitivity regime

The cluster featuring most severe O_3 pollution is C3. Because of its long-lasting high O_3 concentration, over 20 days in total 31 days of C3 experienced MDA8 concentration greater than 100 ppb. The general meteorological conditions, including air temperature and wind are given in Fig. 4. As demonstrated, C3 exhibits a daily temperature-related pattern with high amplitude and a long duration because of the effects of photochemistry and BVOCs (Gu et al., 2020; Sillman and Samson, 1995). The wind direction in the day shifted from southwesterly to southeasterly, and flows from southwest corresponded to ozone pollution time. In order to better understand the potential source region of C3, LPDM simulations were conducted. Compared with C1, air masses of C3 originated mostly from the southwest direction and were transported to Shanghai by southwesterly winds (Fig. 5a–b). To investigate the chemical processes along the transport pathway, the level of total oxidant ($O_x = O_3 + NO_2$) was defined to discern total ozone changes from southeast areas to Shanghai. As shown in Fig. 5c, when air masses transported from Fuyang to Shanghai, O_x gradually rose, and reached its maximum in Shanghai. In the suburb area (Fuyang), though plenty of BVOCs emissions, O_x concentration was still low since that the deficiency of NO_x inhibited ozone production. However, in the urban area (Hangzhou), the concentration of O_x underwent a

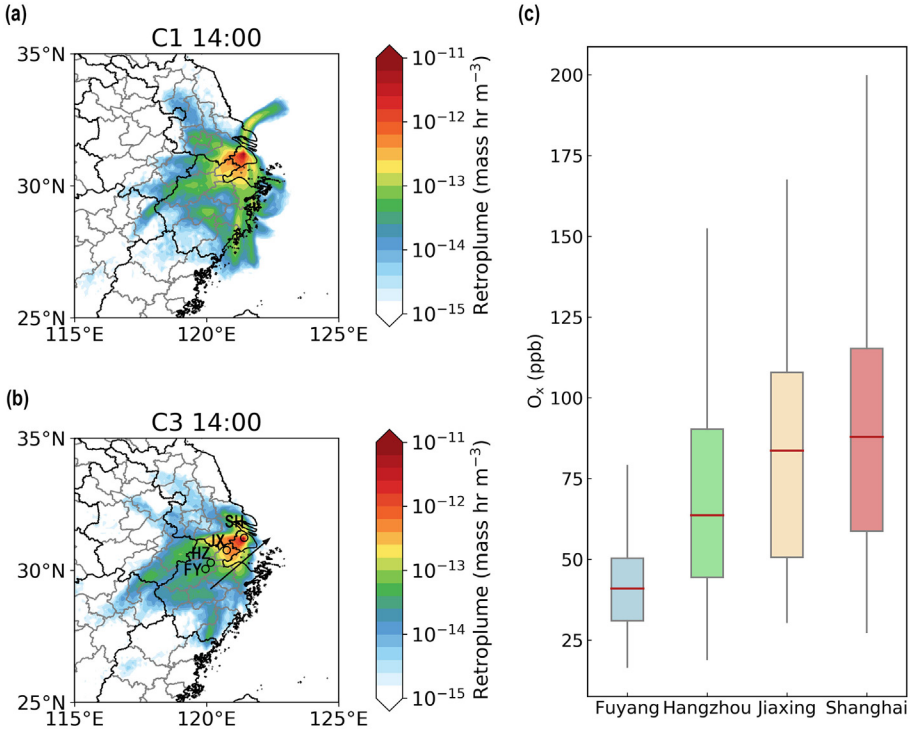

Fig. 5. 24-hour backward trajectories at 100 m based on LPDM of (a) Cluster 1 (C1) and (b) Cluster 3 (C3). The black circles mean locations of representative stations in Shanghai (SH), Jiaxing (JX), Hangzhou (HZ) and Fuyang (FY). (c) Boxplot of O_x of C3 between 8:00 LST to 22:00 LST. Note that the vertical lines for each box correspond to the maximum and minimum values, and the boxes and the horizontal lines mark the 25th, 75th, and 50th percentiles, respectively.

significant increase due to massive NO_x emissions in the city, accompanied by a shift of NO_x-limited regime to transitional regime. Air masses from Hangzhou to downwind regions witnessed transition from sensitivity regime to VOC-limited regime, associated with another O_x rise and then reaching the maximum value in downtown Shanghai. The mixing of BVOCs and anthropogenic pollutants as well as transitions of ozone sensitivity regime along transport could jointly make highly polluted O_3 in C3.

From the retroplume pattern, it could also be noted that some air masses of C1 came from southern areas of Shanghai, in which there was also dense vegetation cover (Fig. 3d). Fig. 6a–b shows the isoprene emissions simulated by MEGAN. The isoprene emission was lower in eastern edge of forest areas and higher around Hangzhou. One likely reason was the difference of plant types. Otherwise, it was calculated that maximum isoprene emission of C3 was 35% higher than that of C1 in suburb Hangzhou, reflecting the difference of other factors between the two clusters, for example, solar radiation and surface temperature. Fig. 6c shows the concentration of HCHO column concentration and the CO surface concentration in Shanghai of C1 and C3. Due to CO and AVOCs are primarily emitted from combustion sources and have good correlation (Baker et al., 2008; Wang et al., 2014), CO is used as a proxy of primary AVOCs, and the similar concentration between C3 and C1 indicated roughly equivalent effect of anthropogenic sources (Atkinson, 2000; Ding et al., 2013b). However, the concentration of HCHO was significantly different, specifically C3 obviously higher than C1. BVOCs emitted from forests would react to produce longer-lived products like HCHO and acetaldehyde (ALD), further to HO_2 radicals (Fu et al., 2007; Geng et al., 2011; Lee et al., 2014). Under the southwest wind regime, HCHO would be transported to regions downwind due to its long lifetime. As a result, Shanghai received more BVOCs and their products of C3. At the same time, winds were required to transport air masses containing supplementary AVOCs and NO_x from industrialized regions. Therefore, the mixed VOCs and NO_x contributed to ozone formation and pollution was intensified in Shanghai.

3.3. Impacts of sea-land breezes on ozone pollution

Apart from magnitude and lasting time of O_3 pollution, it is also worth noting that there exist great disparities in peak hour of O_3 concentration of C2 and C4. Specifically, the peak hour of C4 was around 13:00 LST, whereas in C2 18:00 LST is characterized by highest O_3 level. Such a systematic lag might be linked to diurnal cycles of meteorological conditions. Though regional transport can significantly affect the level of ozone concentration, SLB also exerts great impact on O_3 variation for daily timescale, given the geophysical location of Shanghai. Fig. 7 shows the typical ozone and wind field before and after peak time in Shanghai region. Before reaching ozone peak, sea breeze first appeared around the coastline. At this time, the wind patterns in inland areas were still characterized by southwest winds, and airflows can transport pollutants from the southwest. After the peak of ozone pollution, sea breeze developed and penetrated inland, causing domination of southeast flows in the breeze regime. It was notable that the penetration of sea breeze to urban area was lagging behind the coast for several hours, while the pollution was concentrated in the downtown area.

Wind observations of three meteorological sites were collected to present the evolution of SLB. They are Baoshan (BS) site in the north, Minhang (MH) site in the southwest and Nanhui (NH) site in the southeast of Jing'an station as that marked in Fig. 7. The breeze around the city had a strong convergence trend during period of pollution time, then the ozone concentration began to decrease after the onshore wind penetrated to the urban area (Fig. 8). The prevailing winds at NH site were from southwest, and it was influenced by mixed VOCs mentioned in Section 3.1. In this way the air masses from the southwest with high BVOC level would concentrate near Shanghai. Together with the accumulation and uplift of locally-emitted urban pollutants caused by the strong convergence, ozone production was substantially enhanced. Furthermore, according to Wang et al. (2019), ozone chemical sensitivity tends to experience a shift from VOC-limited to transitional regime in the afternoon in the YRD region, which would further promote the production of O_3 in C2. After the penetration of sea breeze, the state of

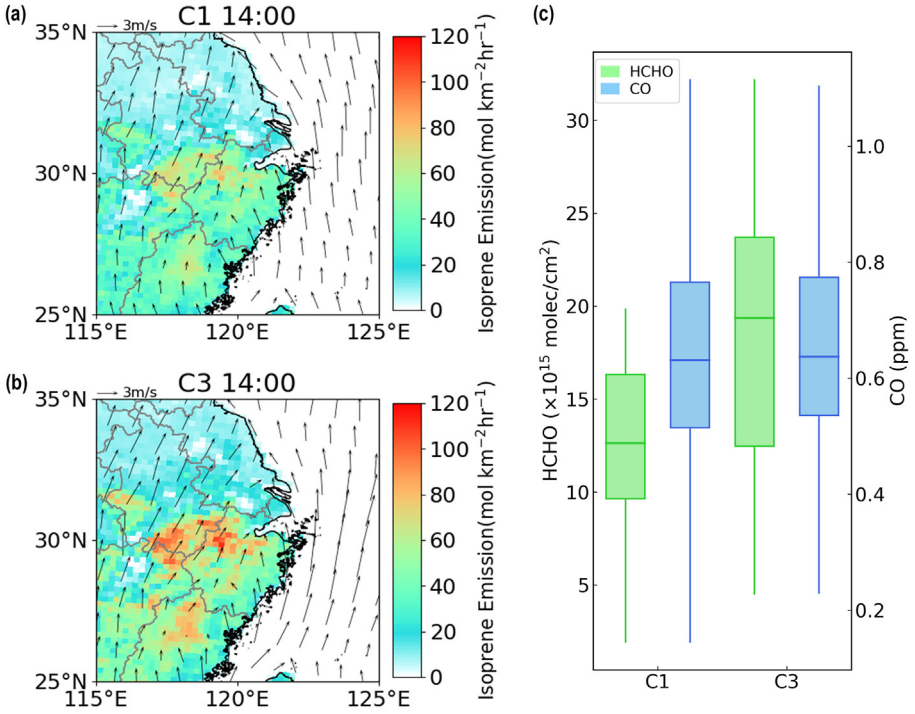

Fig. 6. Averaged modeled isoprene emission and wind fields at 14:00 on (a) C1 and (b) C3 days. (c) Satellite-detected column concentration of HCHO and surface concentration of CO in Shanghai on C1 and C3 days. Note that the vertical lines for each box correspond to the maximum and minimum values, and the boxes and the horizontal lines mark the 25th, 75th, and 50th percentiles, respectively.

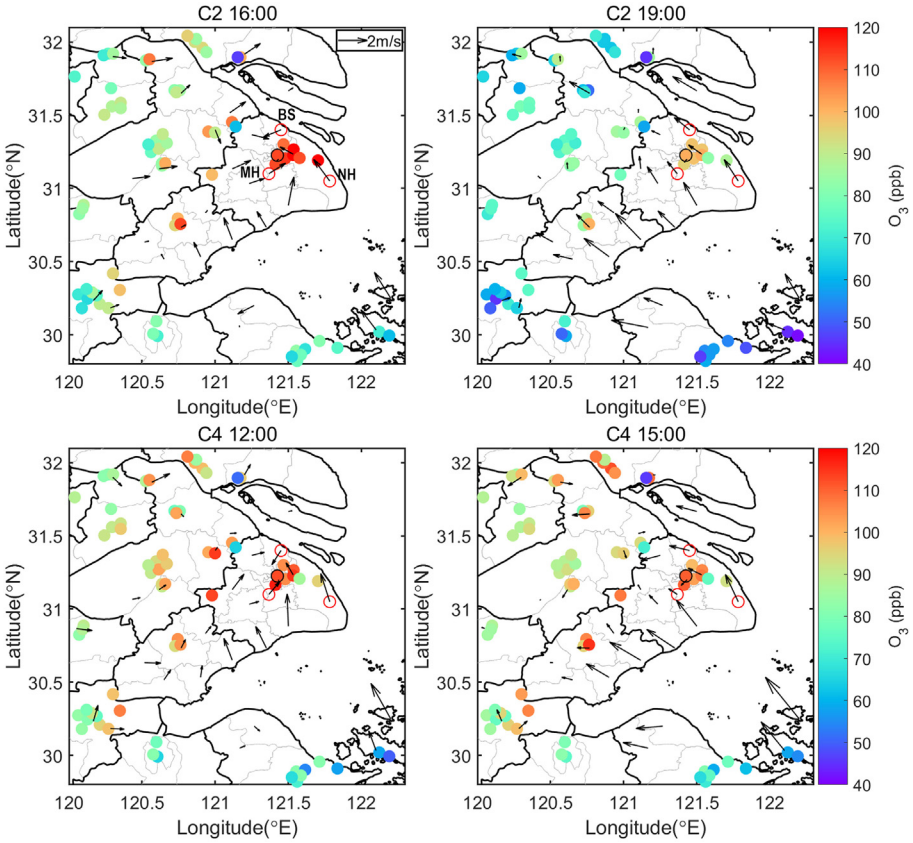

Fig. 7. Ozone and wind of Cluster 2 (C2) and Cluster 4 (C4) before and after ozone peak. Note that air-quality monitoring stations and meteorological stations locate at different places. The three red circles represent Baoshan (BS), Nanhui (NH) and Minhang (MH) meteorological stations while the black circle represents Jing'an station.

convergence was broken, and the ozone in the urban area was transported downwind. Sea breeze would lead to a decrease to the concentration of ozone, but the convergent breeze regime formed under SLB conditions was beneficial to the accumulation and growth of ozone.

The formation of SLB conditions was related to weather background and temperature difference between sea and land. When the subtropical high was enhanced, the miso-scale circulation would generate stronger wind speeds, making SLB harder to form. At the same time, the downdraft flow within the Pacific high would also suppress the updraft from convergence center when sea breeze developed (Tie et al., 2009). Therefore, weak background wind regimes and strong sea-land temperature difference appear to strengthen SLB circulation. Fig. 9a shows the mean sea level pressure at 10:00 LST of C2 and C4. It could be seen that the Pacific High of C2 was stronger. There were low pressure activities caused by typhoons in the West Pacific of C4, making the Pacific High weaker than that of C2. We counted that C4 had typhoon activities in half days and low pressure activities in more than 80% of days in West Pacific (120°E–140°E, 10°N–30°N), which pushed the high pressure northward. On the contrary, typhoons occurred only two

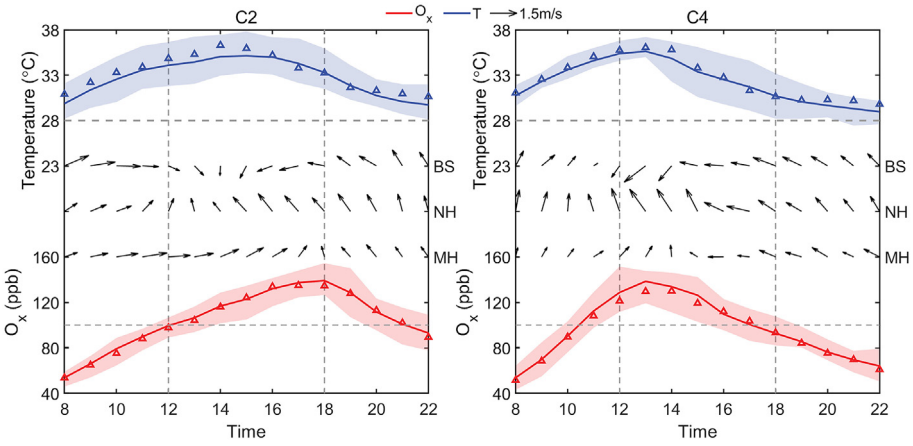

Fig. 8. Time series of temperature, wind and O_x of C2 and C4 in Shanghai. The temperature data comes from downtown Xujiahui site while the wind data comes from Baoshan, Nanhui and Minhang site. The O_x data are for the Jing'an site. Solid lines, triangles and shadows represent mean values, median values and 25th and 75th percentiles respectively.

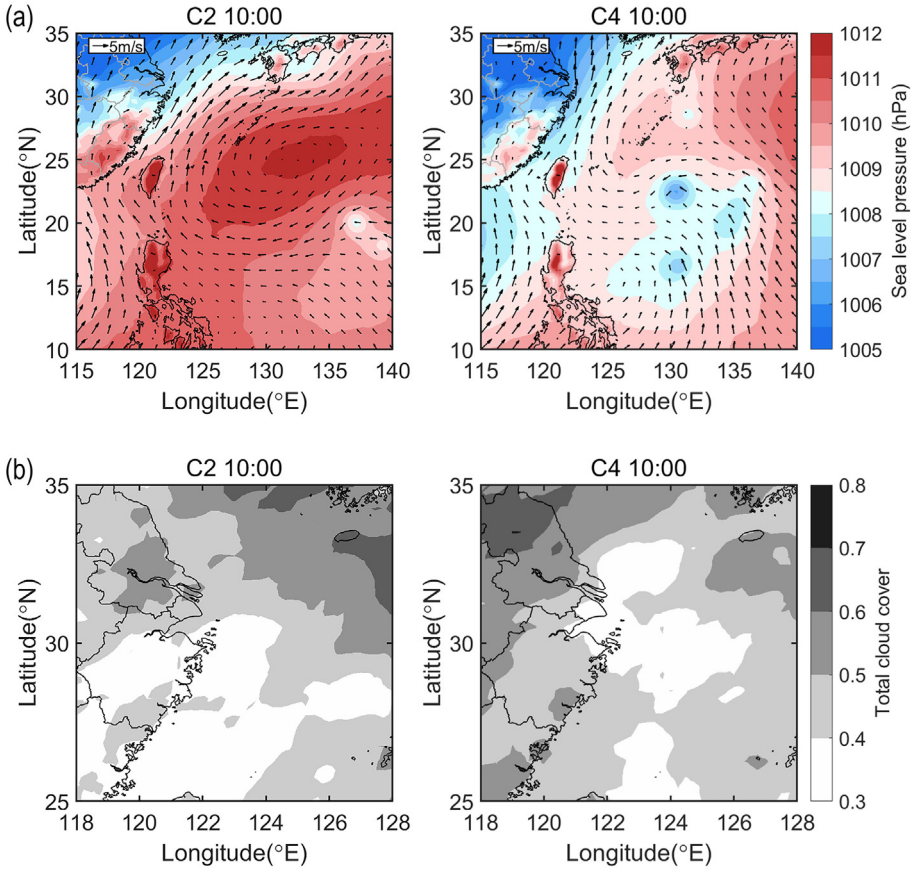

Fig. 9. (a) Sea level pressure and 10 m wind and (b) total cloud cover in the eastern China and West Pacific for the C2 and C4 O_3 diurnal pattern. Note: Figures are plotted based on the ERA5 data.

days in C2. As a result, the large-scale wind field in C4 was weaker, a significantly good sign for the formation of SLBs. Meanwhile, as the high pressure moved northward, the areas with less cloud cover also moved northward (Fig. 9b). It was calculated that average total cloud cover of C4 dropped 28% at 10:00 LST in Shanghai compared with that of C2. As Shanghai got more short-wave radiation, temperature rose earlier and faster, so as to the promotion of temperature difference between sea and land. In the end, the SLB in C4 occurred earlier.

As the above analysis showed, smaller amount of cloud made C4 have more short-wave radiation reaching the surface. It was confirmed in Fig. 10a that the downward UV radiation in Shanghai of C4 was 8%–13% higher, strengthening the intensity of ozone photoreaction. As a result, ozone concentration rose faster from 10:00 LST to 12:00 LST. With the development of SLB circulation, the near-shore convection had caused the cloud cover of C4 to increase. In the afternoon, total cloud cover of C4 reached a similar value with C2 (Fig. 10b), so as to short-wave radiation. Therefore, solar radiation and precursors were vital in ozone production and SLB circulation (Papanastasiou and Melas, 2009). It was worth noting that the development time of SLB circulation was consistent with ozone pollution because of the increase in radiation. In addition, since SLB circulations is not that strong in June and the effect of Meiyu front, it could be explained why C2 and C4 occurred less around this period (Shu et al., 2020).

4. Conclusion

Ozone pollution is one of the main environmental challenge facing the YRD region. This paper provides a new perspective for understanding mechanism of ozone diurnal cycle. A clustering method has been performed to analyze the ozone pollution events in Shanghai. Four main diurnal patterns were identified. Among them, C1 and C3 showed a similar diurnal variation, while the pollution duration of C3 lasted for a longer time. The peak time of C2 was around sunset, and C4 went ozone pollution earlier.

Combined with meteorological conditions, two main conclusions were drawn. First, ozone pollution could be intensified due to regional transport of BVOCs and the transition in chemical sensitivity regime. With the influence of the subtropical high, the prevailing winds in Shanghai were from southwest. Even under a similar level of primary pollution, the concentrations of ozone pollution can differ a lot because different air masses from forest area with high BVOCs and those from urban areas. At the same time, mixed-VOCs airflows underwent a transition from the NO_x-limited regime to the VOC-limited regime when reaching Shanghai, which also increased ozone concentration. Second, SLB circulation can significantly influence summer ozone pollution in the YRD region. When there were typhoon activities in Western Pacific, high pressure and areas of low cloud cover moved north, making total cloud cover 20%–30% less and solar radiation 8%–13% more than general days in Shanghai, promoting ozone production in the morning. Meanwhile, strong radiation enhanced the increase of land temperature and land-sea temperature difference, which accelerated SLB circulation. When offshore wind turned to onshore wind, a convergent breeze regime was formed in Shanghai, which was also favorable for the production and accumulation of ozone. Therefore, the ozone pollution time coincided well with the development of sea breeze. After the penetration of sea breeze reached inland, ozone was transported to downwind areas, leading a rapid drop in O_3 concentration.

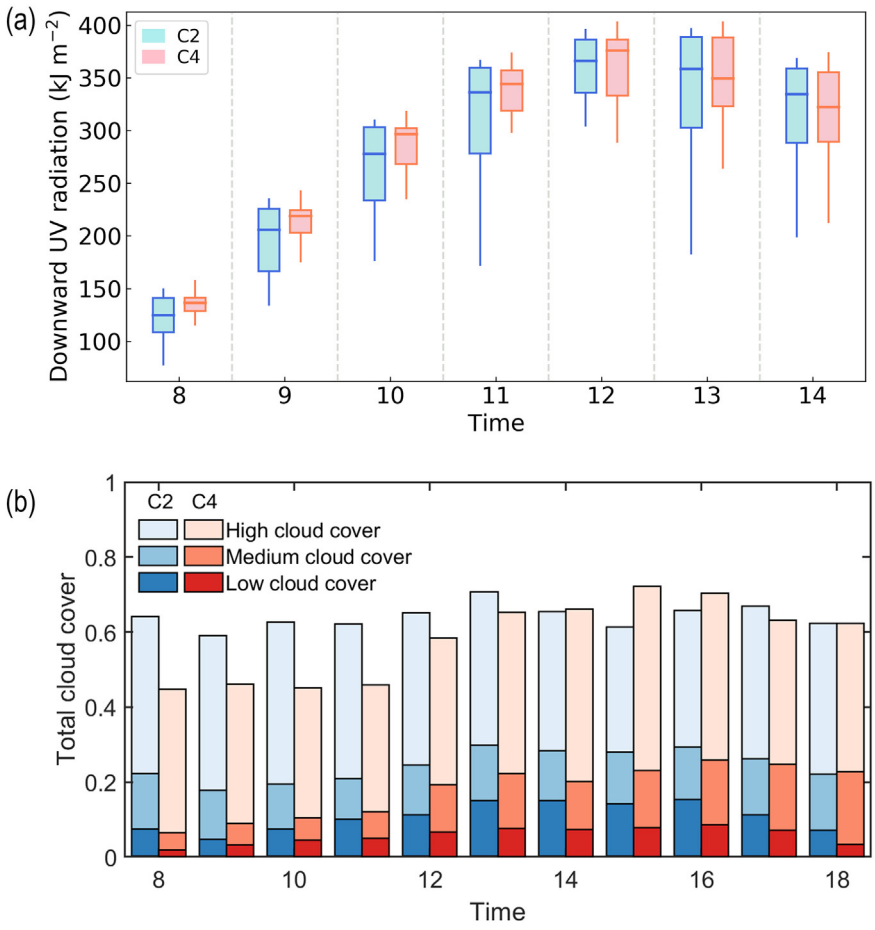

Fig. 10. (a) Ensembled diurnal patterns of downward short-wave radiation in Shanghai. The boxplot lines were defined in Fig. 2. (b) Changes of low, median and high cloud cover based on ERA5 data.

This work comprehensively analyzed ozone pollution in Shanghai from the perspective of its diurnal cycles. Both photochemical production and regional transport for different pollution kinds are studies in detail. We indicated that in the YRD region, despite of intensive anthropogenic activities, biogenic emissions also play a significant role in vigorous chemical O_3 production. Favorable synoptic conditions like prevailing southwest wind favor the mix of biogenic and anthropogenic precursors, and subsequently enhanced O_3 production due to the transition of sensitivity regime. Meanwhile, we also found that the peak and lasting time of O_3 pollution in Shanghai, as a typical coastal city, also highly depend on the evolution of SLB. Though plenty of emission control measures of fossil fuel combustion have been implemented to mitigate ozone pollution in Shanghai and YRD, the importance of biogenic contribution and SLB still need to be highlighted.

CRediT authorship contribution statement

Jiawei Xu: Formal analysis, Data curation, Methodology, Visualization, Writing - review & editing. **Xin Huang:** Methodology, Investigation, Writing - review & editing. **Nan Wang:** Formal analysis. **Yuanyuan Li:** Methodology. **Aijun Ding:** Conceptualization, Supervision, Funding acquisition, Writing - review & editing.

Declaration of competing interest

The authors declare that they have no known competing financial interests or personal relationships that could have appeared to influence the work reported in this paper.

Acknowledgements

This work was supported by the Ministry of Science and Technology of the People's Republic of China (2016YFC0200500, 2018YFC0213800) and the National Natural Science Foundation of China (41725020, 91744311, 41922038). Real-time air quality data across China were collected through the online access to ambient air monitoring data center (http://datacenter.mee.gov.cn). The ERA5 reanalysis data is from https://cds.climate.copernicus.eu, and global daily satellite data are available at http://www.temis.nl/index.php.

References

Adame, J.A., Bolívar, J.P., de la Morena, B.A., 2010. Surface ozone measurements in the southwest of the Iberian Peninsula (Huelva, Spain). Environ. Sci. Pollut. Res. 17, 355–368. https://doi.org/10.1007/s11356-008-0098-9.

Adame, J.A., Notario, A., Villanueva, F., Albaladejo, J., 2012. Application of cluster analysis to surface ozone, NO2 and SO2 daily patterns in an industrial area in Central-Southern Spain measured with a DOAS system. Sci. Total Environ. 429, 281–291. http://www.sciencedirect.com/science/article/pii/S0048969712005645.

Atkinson, R., 2000. Atmospheric chemistry of VOCs and NOx. Atmos. Environ. 34, 2063–2101. http://www.sciencedirect.com/science/article/pii/S1352231099004604.

Austin, E., Coull, B.A., Zanobetti, A., Koutrakis, P., 2013. A framework to spatially cluster air pollution monitoring sites in US based on the PM2. 5 composition. Environ. Int. 59, 244–254. https://doi.org/10.1016/j.envint.2013.06.003.

Baker, A.K., Beyersdorf, A.J., Doezema, L.A., Katzenstein, A., Meinardi, S., Simpson, I.J., et al., 2008. Measurements of nonmethane hydrocarbons in 28 United States cities. Atmos. Environ. 42, 170–182. http://www.sciencedirect.com/science/article/pii/S1352231007007996.

Boersma, K.F., Eskes, H.J., Brinksma, E.J., 2004. Error analysis for tropospheric NO2 retrieval from space. Journal of Geophysical Research: Atmospheres 109. https://doi.org/10.1029/2003JD003962.

Bosson, J., Pourazar, J., Forsberg, B., Ädelroth, E., Sandström, T., Blomberg, A., 2007. Ozone enhances the airway inflammation initiated by diesel exhaust. Respir. Med. 101, 1140–1146. http://www.sciencedirect.com/science/article/pii/S095461110600597X.

Bouchlaghem, K., Mansour, F.B., Elouragini, S., 2007. Impact of a sea breeze event on air pollution at the Eastern Tunisian Coast. Atmos. Res. 86, 162–172. http://www.sciencedirect.com/science/article/pii/S0169809507000683.

Brauer, M., Freedman, G., Frostad, J., van Donkelaar, A., Martin, R.V., Dentener, F., et al., 2016. Ambient air pollution exposure estimation for the Global Burden of Disease 2013. Environmental Science & Technology 50, 79–88. https://doi.org/10.1021/acs.est.5b03709.

Buckley, R.D., Hackney, J.D., Clark, K., Posin, C., 1975. Ozone and human blood. Archives of Environmental Health: An International Journal 30, 40–43. https://doi.org/10.1080/00039896.1975.10666631.

Chameides, W.L., Fehsenfeld, F., Rodgers, M.O., Cardelino, C., Martinez, J., Parrish, D., et al., 1992. Ozone precursor relationships in the ambient atmosphere. Journal of Geophysical Research: Atmospheres 97, 6037–6055. https://doi.org/10.1029/91JD03014.

Choi, Y., Kim, H., Tong, D., Lee, P., 2012. Summertime weekly cycles of observed and modeled NO_x and O_3 concentrations as a function of satellite-derived ozone production sensitivity and land use types over the Continental United States. Atmos. Chem. Phys. 12, 6291–6307. https://acp.copernicus.org/articles/12/6291/2012/.

Cooper, O.R., Parrish, D.D., Stohl, A., Trainer, M., Nédélec, P., Thouret, V., et al., 2010. Increasing springtime ozone mixing ratios in the free troposphere over western North America. Nature 463, 344. https://doi.org/10.1038/nature08708.

De Smedt, I., Müller, J.F., Stavrakou, T., van der, A.R., Eskes, H., Van Roozendael, M., 2008. Twelve years of global observations of formaldehyde in the troposphere using GOME and SCIAMACHY sensors. Atmos. Chem. Phys. 8, 4947–4963. https://www.atmos-chem-phys.net/8/4947/2008/.

Ding, A., Wang, T., Zhao, M., Wang, T., Li, Z., 2004. Simulation of sea-land breezes and a discussion of their implications on the transport of air pollution during a multi-day ozone episode in the Pearl River Delta of China. Atmos. Environ. 38, 6737–6750. http://www.sciencedirect.com/science/article/pii/S1352231004008581.

Ding, A., Wang, T., Fu, C., 2013a. Transport characteristics and origins of carbon monoxide and ozone in Hong Kong, South China. Journal of Geophysical Research: Atmospheres 118, 9475–9488. https://doi.org/10.1002/jgrd.50714.

Ding, A.J., Fu, C.B., Yang, X.Q., Sun, J.N., Zheng, L.F., Xie, Y.N., et al., 2013b. Ozone and fine particle in the western Yangtze River Delta: an overview of 1 yr data at the SORPES station. Atmos. Chem. Phys. 13, 5813–5830. https://www.atmos-chem-phys.net/13/5813/2013/.

Ding, A., Huang, X., Nie, W., Chi, X., Xu, Z., Zheng, L., et al., 2019. Significant reduction of PM2.5 in eastern China due to regional-scale emission control: evidence from SORPES in 2011–2018. Atmos. Chem. Phys. 19, 11791–11801. https://www.atmos-chem-phys.net/19/11791/2019/.

Domínguez-López, D., Adame, J.A., Hernández-Ceballos, M.A., Vaca, F., De la Morena, B.A., Bolívar, J.P., 2014. Spatial and temporal variation of surface ozone, NO and NO2 at urban, suburban, rural and industrial sites in the southwest of the Iberian Peninsula. Environ. Monit. Assess. 186, 5337–5351. https://doi.org/10.1007/s10661-014-3783-9.

Draxier, R.R., Hess, G.D., 1998. An overview of the HYSPLIT_4 modeling system of trajectories, dispersion, and deposition. Aust. Meteorol. Mag. 47, 295–308.

Duncan, B.N., Yoshida, Y., Olson, J.R., Sillman, S., Martin, R.V., Lamsal, L., et al., 2010. Application of OMI observations to a space-based indicator of NOx and VOC controls on surface ozone formation. Atmos. Environ. 44, 2213–2223. http://www.sciencedirect.com/science/article/pii/S1352231010002050.

Everitt, B.S., Landau, S., Leese, M., Stahl, D., 2011. Cluster Analysis. John Wiley & Sons, London.

Fu, Y., Liao, H., 2012. Simulation of the interannual variations of biogenic emissions of volatile organic compounds in China: impacts on tropospheric ozone and secondary organic aerosol. Atmos. Environ. 59, 170–185. http://www.sciencedirect.com/science/article/pii/S1352231012005304.

Fu, T.-M., Jacob, D.J., Palmer, P.I., Chance, K., Wang, Y.X., Barletta, B., et al., 2007. Space-based formaldehyde measurements as constraints on volatile organic compound emissions in east and South Asia and implications for ozone. Journal of Geophysical Research: Atmospheres 112. https://doi.org/10.1029/2006JD007853.

Geng, F., Tie, X., Xu, J., Zhou, G., Peng, L., Gao, W., et al., 2008. Characterizations of ozone, NOx, and VOCs measured in Shanghai, China. Atmos. Environ. 42, 6873–6883. http://www.sciencedirect.com/science/article/pii/S1352231008005323.

Geng, F., Tie, X., Guenther, A., Li, G., Cao, J., Harley, P., 2011. Effect of isoprene emissions from major forests on ozone formation in the city of Shanghai, China. Atmos. Chem. Phys. 11, 10449–10459. https://www.atmos-chem-phys.net/11/10449/2011/.

Grell, G.A., Peckham, S.E., Schmitz, R., McKeen, S.A., Frost, G., Skamarock, W.C., et al., 2005. Fully coupled "online" chemistry within the WRF model. Atmos. Environ. 39, 6957–6975. http://www.sciencedirect.com/science/article/pii/S1352231005003560.

Gu, Y., Li, K., Xu, J., Liao, H., Zhou, G., 2020. Observed dependence of surface ozone on increasing temperature in Shanghai, China. Atmos. Environ. 221, 117108. http://www.sciencedirect.com/science/article/pii/S1352231019307472.

Guenther, A., Karl, T., Harley, P., Wiedinmyer, C., Palmer, P.I., Geron, C., 2007. Estimates of global terrestrial isoprene emissions using MEGAN (Model of Emissions of Gases and Aerosols from Nature). Atmos. Chem. Phys. 7, 4327. https://www.atmos-chem-phys.net/6/3181/2006/.

He, J., Wang, Y., Hao, J., Shen, L., Wang, L., 2012. Variations of surface O3 in August at a rural site near Shanghai: influences from the West Pacific subtropical high and anthropogenic emissions. Environ. Sci. Pollut. Res. 19, 4016–4029. https://doi.org/10.1007/s11356-012-0970-5.

Huang, R.-J., Zhang, Y., Bozzetti, C., Ho, K.-F., Cao, J.-J., Han, Y., et al., 2014. High secondary aerosol contribution to particulate pollution during haze events in China. Nature 514, 218. https://doi.org/10.1038/nature13774.

Huang, X., Zhou, L., Ding, A., Qi, X., Nie, W., Wang, M., et al., 2016. Comprehensive modelling study on observed new particle formation at the SORPES station in Nanjing, China. Atmos. Chem. Phys. 16, 2477–2492. https://www.atmos-chem-phys.net/16/2477/2016/.

Huang, X., Ding, A., Gao, J., Zheng, B., Zhou, D., Qi, X., et al., 2020a. Enhanced secondary pollution offset reduction of primary emissions during COVID-19 lockdown in China. Natl. Sci. Rev. https://doi.org/10.1093/nsr/nwaa137.

Huang, X., Ding, A., Wang, Z., Ding, K., Gao, J., Chai, F., et al., 2020b. Amplified transboundary transport of haze by aerosol–boundary layer interaction in China. Nat. Geosci. 13, 428–434. https://doi.org/10.1038/s41561-020-0583-4.

IPCC, 2013. Intergovernmental Panel in Climate Change (IPCC). Press CU, Cambridge, U.K., and New York.

Jiang, F., Wang, T., Wang, T., Xie, M., Zhao, H., 2008. Numerical modeling of a continuous photochemical pollution episode in Hong Kong using WRF–chem. Atmos. Environ. 42, 8717–8727. http://www.sciencedirect.com/science/article/pii/S1352231008008042.

Jin, X., Holloway, T., 2015. Spatial and temporal variability of ozone sensitivity over China observed from the Ozone Monitoring Instrument. Journal of Geophysical Research: Atmospheres 120, 7229–7246. https://doi.org/10.1002/2015JD023250.

Jin, L., Harley, R.A., Brown, N.J., 2011. Ozone pollution regimes modeled for a summer season in California's San Joaquin Valley: a cluster analysis. Atmos. Environ. 45, 4707–4718. http://www.sciencedirect.com/science/article/pii/S1352231011004535.

Jin, X., Fiore, A.M., Murray, L.T., Valin, L.C., Lamsal, L.N., Duncan, B., et al., 2017. Evaluating a space-based indicator of surface ozone-NOx-VOC sensitivity over midlatitude source regions and application to decadal trends. Journal of Geophysical Research: Atmospheres 122, 10,439–10,461. https://doi.org/10.1002/2017JD026720.

Klemm, O., Ziomas, I.C., Balis, D., Suppan, P., Slemr, J., Romero, R., et al., 1998. A summer air-pollution study in Athens, Greece. Atmos. Environ. 32, 2071–2087. http://www.sciencedirect.com/science/article/pii/S135223109700424X.

Kong, L., Du, C., Zhanzakova, A., Cheng, T., Yang, X., Wang, L., et al., 2018. Trends in heterogeneous aqueous reaction in continuous haze episodes in suburban Shanghai: an in-depth case study. Sci. Total Environ. 634, 1192–1204. https://doi.org/10.1016/j.scitotenv.2018.04.086.

Lasry, F., Coll, I., Buisson, E., 2005. An insight into the formation of severe ozone episodes: modeling the 21/03/01 event in the ESCOMPTE region. Atmos. Res. 74, 191–215. http://www.sciencedirect.com/science/article/pii/S0169809504001516.

Lee, K.-Y., Kwak, K.-H., Ryu, Y.-H., Lee, S.-H., Baik, J.-J., 2014. Impacts of biogenic isoprene emission on ozone air quality in the Seoul metropolitan area. Atmos. Environ. 96, 209–219. http://www.sciencedirect.com/science/article/pii/S1352231014005664.

Lelieveld, J., van Aardenne, J., Fischer, H., de Reus, M., Williams, J., Winkler, P., 2004. Increasing ozone over the Atlantic Ocean. Science 304, 1483. http://science.sciencemag.org/content/304/5676/1483.abstract.

Li, L., Chen, C., Huang, C., Huang, H., Zhang, G., Wang, Y., et al., 2011. Ozone sensitivity analysis with the MM5-CMAQ modeling system for Shanghai. J. Environ. Sci. 23, 1150–1157. http://www.sciencedirect.com/science/article/pii/S100107421060527X.

Li, H., Li, L., Huang, C., An, J.-y., Yan, R.-s., Huang, H.-y., et al., 2015. Ozone source apportionment at urban area during a typical photochemical pollution episode in the summer of 2013 in the Yangtze River Delta. Environmental Science 36, 1–10. http://europepmc.org/abstract/MED/25898640.

Li, L., An, J.Y., Shi, Y.Y., Zhou, M., Yan, R.S., Huang, C., et al., 2016. Source apportionment of surface ozone in the Yangtze River Delta, China in the summer of 2013. Atmos. Environ. 144, 194–207. http://www.sciencedirect.com/science/article/pii/S1352231016306823.

Li, K., Jacob, D.J., Liao, H., Shen, L., Zhang, Q., Bates, K.H., 2018. Anthropogenic drivers of 2013–2017 trends in summer surface ozone in China. Proc. Natl. Acad. Sci. 116, 422–427. https://www.pnas.org/content/pnas/early/2018/12/26/1812168116.full.pdf.

Liu, K.-Y., Wang, Z., Hsiao, L.-F., 2002. A modeling of the sea breeze and its impacts on ozone distribution in northern Taiwan. Environ. Model Softw. 17, 21–27. http://www.sciencedirect.com/science/article/pii/S1364815201000494.

Liu, Y., Li, L., An, J., Huang, L., Yan, R., Huang, C., et al., 2018. Estimation of biogenic VOC emissions and its impact on ozone formation over the Yangtze River Delta region, China. Atmos. Environ. 186, 113–128. http://www.sciencedirect.com/science/article/pii/S1352231018303303.

MacQueen, J., 1967. Some methods for classification and analysis of multivariate observations. Berkley: Proceedings of the Fifth Berkeley Symposium on Mathematical Statistics and Probability. vol 1.

Mangia, C., Schipa, I., Tanzarella, A., Conte, D., Marra, G.P., Marcello Miglietta, M., et al., 2010. A numerical study of the effect of sea breeze circulation on photochemical pollution over a highly industrialized peninsula. Meteorol. Appl. 17, 19–31. https://doi.org/10.1002/met.147.

Martin, R.V., Fiore, A.M., Donkelaar, A.V., 2004. Space-based diagnosis of surface ozone sensitivity to anthropogenic emissions. Geophys. Res. Lett. 31, 337–357. https://doi.org/10.1029/2004GL019416.

Meleux, F., Solmon, F., Giorgi, F., 2007. Increase in summer European ozone amounts due to climate change. Atmos. Environ. 41, 7577–7587. http://www.sciencedirect.com/science/article/pii/S1352231007004980.

Ming, L., Jin, L., Li, J., Fu, P., Yang, W., Liu, D., et al., 2017. $PM_{2.5}$ in the Yangtze River Delta, China: chemical compositions, seasonal variations, and regional pollution events. Environ. Pollut. 223, 200–212. http://www.sciencedirect.com/science/article/pii/S0269749117300970.

Papanastasiou, D., Melas, D., 2009. Climatology and impact on air quality of sea breeze in an urban coastal environment. International Journal of Climatology: A Journal of the Royal Meteorological Society 29, 305–315. https://doi.org/10.1002/joc.780.

Pathak, R.K., Wu, W.S., Wang, T., 2009. Summertime $PM_{2.5}$ ionic species in four major cities of China: nitrate formation in an ammonia-deficient atmosphere. Atmos. Chem. Phys. 9, 1711–1722. https://www.atmos-chem-phys.net/9/1711/2009/.

Seinfeld, J.H., Pandis, S.N., 2012. Atmospheric Chemistry and Physics: From Air Pollution to Climate Change. John Wiley & Sons, London.
Shu, L., Xie, M., Wang, T., Gao, D., Chen, P., Han, Y., et al., 2016. Integrated studies of a regional ozone pollution synthetically affected by subtropical high and typhoon system in the Yangtze River Delta region. China. Atmospheric Chemistry and Physics 16, 15801–15819. https://doi.org/10.5194/acp-16-15801-2016.
Shu, L., Wang, T., Han, H., Xie, M., Chen, P., Li, M., et al., 2020. Summertime ozone pollution in the Yangtze River Delta of eastern China during 2013–2017: synoptic impacts and source apportionment. Environ. Pollut. 257, 113631. http://www.sciencedirect.com/science/article/pii/S0269749119331094.
Sillman, S., 1995. The use of NO_y, H_2O_2 and HNO_3 as indicators for ozone-NO_x-hydrocarbon sensitivity in urban locations. Journal of Geophysical Research: Atmospheres. 100, 14175–14188. https://doi.org/10.1029/94JD02953.
Sillman, S., He, D., 2002. Some theoretical results concerning O_3-NO_x-VOC chemistry and NO_x-VOC indicators. Journal of Geophysical Research: Atmospheres 107, ACH 26–1-ACH 26-15. https://doi.org/10.1029/2001JD001123.
Sillman, S., Samson, P.J., 1995. Impact of temperature on oxidant photochemistry in urban, polluted rural and remote environments. Journal of Geophysical Research: Atmospheres 100, 11497–11508. https://doi.org/10.1029/94JD02146.
Sillman, S., West, J.J., 2009. Reactive nitrogen in Mexico City and its relation to ozone-precursor sensitivity: results from photochemical models. Atmos. Chem. Phys. 9, 3477–3489. https://www.atmos-chem-phys.net/9/3477/2009/.
Sillman, S., Vautard, R., Menut, L., Kley, D., 2003. O3-NOx-VOC sensitivity and NOx-VOC indicators in Paris: results from models and Atmospheric Pollution Over the Paris Area (ESQUIF) measurements. Journal of Geophysical Research: Atmospheres 108. https://doi.org/10.1029/2002JD001561.
Situ, S., Guenther, A., Wang, X., Jiang, X., Turnipseed, A., Wu, Z., et al., 2013. Impacts of seasonal and regional variability in biogenic VOC emissions on surface ozone in the Pearl River delta region, China. Atmos. Chem. Phys 13, 11803–11817. https://www.atmos-chem-phys.net/13/11803/2013/.
Stauffer, R.M., Thompson, A.M., Martins, D.K., Clark, R.D., Goldberg, D.L., Loughner, C.P., et al., 2015. Bay breeze influence on surface ozone at Edgewood, MD during July 2011. J. Atmos. Chem. 72, 335–353. https://doi.org/10.1007/s10874-012-9241-6.
Stein, A.F., Draxler, R.R., Rolph, G.D., Stunder, B.J.B., Cohen, M.D., Ngan, F., 2016. NOAA's HYSPLIT atmospheric transport and dispersion modeling system. Bull. Am. Meteorol. Soc. 96, 2059–2077. https://doi.org/10.1175/BAMS-D-14-00110.1.
Tager, I.B., John, B., Frederick, L., Long, N., Siana, A., Nino, K.J.E., 2005. Chronic exposure to ambient ozone and lung function in young adults. Epidemiology 16, 751–759. https://doi.org/10.1097/01.ede.0000183166.68809.b0.
Tie, X., Geng, F., Peng, L., Gao, W., Zhao, C., 2009. Measurement and modeling of O_3 variability in Shanghai, China: application of the WRF-Chem model. Atmos. Environ. 43, 4289–4302. https://doi.org/10.1016/j.atmosenv.2009.06.008.
Tie, X., Geng, F., Guenther, A., Cao, J., Greenberg, J., Zhang, R., et al., 2013. Megacity impacts on regional ozone formation: observations and WRF-Chem modeling for the MIRAGE-Shanghai field campaign. Atmos. Chem. Phys. 13, 5655–5669. https://www.atmos-chem-phys.net/13/5655/2013/.
Uysal, N., Schapira, R.M., 2003. Effects of ozone on lung function and lung diseases. Curr. Opin. Pulm. Med. 9. https://journals.lww.com/co-pulmonarymedicine/Fulltext/2003/03000/Effects_of_ozone_on_lung_function_and_lung.9.aspx.
Vargas, A., Arnold, D., Adame, J.A., Grossi, C., Hernández-Ceballos, M.A., Bolivar, J.P., 2015. Analysis of the vertical radon structure at the Spanish "El Arenosillo" tower station. J. Environ. Radioact. 139, 1–17. http://www.sciencedirect.com/science/article/pii/S0265931X14002847.
Wang, M., Shao, M., Chen, W., Yuan, B., Lu, S., Zhang, Q., et al., 2014. A temporally and spatially resolved validation of emission inventories by measurements of ambient volatile organic compounds in Beijing. China. Atmos. Chem. Phys 14, 5871–5891. https://acp.copernicus.org/articles/14/5871/2014/.
Wang, T., Xue, L., Brimblecombe, P., Lam, Y.F., Li, L., Zhang, L., 2017. Ozone pollution in China: a review of concentrations, meteorological influences, chemical precursors, and effects. Sci. Total Environ. 575, 1582–1596. http://www.sciencedirect.com/science/article/pii/S0048969716322471.
Wang, N., Lyu, X., Deng, X., Huang, X., Jiang, F., Ding, A., 2019. Aggravating O_3 pollution due to NO_x emission control in eastern China. Sci. Total Environ. 677, 732–744. http://www.sciencedirect.com/science/article/pii/S0048969719319333.
Wang, Y., Gao, W., Wang, S., Song, T., Gong, Z., Ji, D., et al., 2020. Contrasting trends of PM2.5 and surface-ozone concentrations in China from 2013 to 2017. Natl. Sci. Rev. 7, 1331–1339. https://doi.org/10.1093/nsr/nwaa032.
Wei, X.L., Li, Y.S., Lam, K.S., Wang, A.Y., Wang, T.J., 2007. Impact of biogenic VOC emissions on a tropical cyclone-related ozone episode in the Pearl River Delta region, China. Atmos. Environ. 41, 7851–7864. http://www.sciencedirect.com/science/article/pii/S1352231007005614.
Xu, Z., Huang, X., Nie, W., Chi, X., Xu, Z., Zheng, L., et al., 2017. Influence of synoptic condition and holiday effects on VOCs and ozone production in the Yangtze River Delta region, China. Atmos. Environ. 168, 112–124. http://www.sciencedirect.com/science/article/pii/S1352231017305496.
Xu, J., Tie, X., Gao, W., Lin, Y., Fu, Q., 2019. Measurement and model analyses of the ozone variation during 2006 to 2015 and its response to emission change in megacity Shanghai, China. Atmos. Chem. Phys. 19, 9017–9035. https://www.atmos-chem-phys.net/19/9017/2019/.
Xue, L., Ding, A., Cooper, O., Huang, X., Wang, W., Zhou, D., et al., 2020. ENSO and Southeast Asian biomass burning modulate subtropical trans-Pacific ozone transport. Natl. Sci. Rev. https://doi.org/10.1093/nsr/nwaa132.
Zhang, Y., Mao, H., Ding, A., Zhou, D., Fu, C., 2013. Impact of synoptic weather patterns on spatio-temporal variation in surface O3 levels in Hong Kong during 1999–2011. Atmos. Environ. 73, 41–50. http://www.sciencedirect.com/science/article/pii/S1352231013001593.
Zhang, Q., Yuan, B., Shao, M., Wang, X., Lu, S., Lu, K., et al., 2014. Variations of ground-level O_3 and its precursors in Beijing in summertime between 2005 and 2011. Atmos. Chem. Phys. 14, 6089–6101. https://www.atmos-chem-phys.net/14/6089/2014/.
Zhang, Y., Ding, A., Mao, H., Nie, W., Zhou, D., Liu, L., et al., 2016. Impact of synoptic weather patterns and inter-decadal climate variability on air quality in the North China Plain during 1980–2013. Atmos. Environ. 124, 119–128. http://www.sciencedirect.com/science/article/pii/S1352231015301345.
Zhang, Q., Zheng, Y., Tong, D., Shao, M., Wang, S., Zhang, Y., et al., 2019. Drivers of improved $PM_{2.5}$ air quality in China from 2013 to 2017. 116, 24463–24469. https://www.pnas.org/content/pnas/116/49/24463.full.pdf.